Improved Selective Segmentation Model Using One Level-Set

Lavdie Rada and Ke Chen*

Received 31/08/2012; Accepted 04/01/2013

ABSTRACT

Variational segmentation models have proven to be extremely efficient for segmenting and tracking boundaries and in most cases all of the boundaries in an image. Such models are for global segmentation. For a large class of image segmentation tasks where only one object is required to be extracted automatically, global models cannot deliver the solution and we need selective segmentation techniques.

In this paper, we propose a novel, variational and single level-set function for the selective segmentation task. The model is much faster to implement than the previously dual level set model by Rada-Chen [29] by having the same efficiency and reliability. In comparing with interactive image segmentation algorithm of Nguyen-Cai-Zhang-Zheng method [2], our model shows some improvement in some cases. Several new ideas are incorporated in this new work: i) the distance function is only needed optionally and its inclusion does not affect the result; ii) an adaptive parameter is introduced in the edge detection function; iii) a new area-based fitting term is added to enhance the model's reliability (different from the idea of minimizing the area of the object). We develop an additive operator splitting method for solving the resulting Euler-Lagrange equation.

Test results show that the new model finds the desired local boundaries successfully in various challenging cases and indeed it is not much dependent on the prior information of markers or the distance function based on them. More importantly, the new model gives an overall improvement over the previous models and can be recommended for selective segmentation.

AMS subject classification: 62H35, 65N22, 68U10, 35A15, 65C20, 74G65, 74G75.

Keywords: Image processing, Image selective segmentation, Total variation, Level set function, Edge detection, 2D image segmentation, Euler-Lagrange equation.

*Both authors are with Centre for Mathematical Imaging Techniques and Department of Mathematical Sciences, The University of Liverpool, United Kingdom. Corresponding author's email k.chen@liv.ac.uk, Web: http://www.liv.ac.uk/cmit

1. INTRODUCTION

The progress in photography, imaging instruments, high resolution magnetic resonance and the access to the three dimensional imaging has already provided a lot of valuable information in different fields. Despite developments and improvements in the technology a post process is required in order to separate the objects from their surroundings. This procedure is referred to as "segmentation" and different techniques have been developed so far, such as histogram analysis and thresholding [24, 32, 37], region growing [1, 42], edge detection and active contours [3, 10, 20], etc. Of all these techniques, variational techniques [9, 26, 28] are proven to be very efficient for extracting homogenous areas compared with other models such as statistical methods [32, 11, 13, 40] or wavelet techniques [19, 25, 35].

Most segmentation approaches from the last two decades can be put into two important categories of segmentation methods: edge-based and region-based methods. Of course, one may develop a hybrid method. Edge-based methods refer to methods which drive the contours towards image edges using an edge detector function. The "snake" algorithm by Kass *et al*. [20] was the first variational method for object segmentation in images. Further development of the "snake" algorithm was the Geodesic Active Contours model and the level-set method have proven to be effective for such a model [3, 33, 7, 31]. Most models use an edge detector function which depends on the gradient of a given image [7, 16, 18] such as $g(\left|\nabla u_0\right|) = \dfrac{1}{1+\left|\nabla u_0\right|^p}, p \geq 1,$ where $u_0 = u_0(x, y)$ (in 2-D case) defines the given image.

On the other hand, among region-based methods such as minimum description length criteria [21], region growing and emerging [1], watershed algorithms [37] etc., Mumford-Shah functional minimization [26] was found to be the most efficient for the images with and without noise. It reconstructs the image as a piecewise continuous function that is surrounded by discontinuities represented by contours. For a given image u_0 defined on a rectangular domain Ω, Mumford-Shah [26] general model was reduced and converted to an easy numerical represented model by Chan-Vese (CV) [9]. This model is a special case of the piecewise constant where Mumford-Shah is restricted to only two phases, representing the foreground and the background of the image. The method was further extended for multiphases and for an phase number automatically determined [9, 8, 10, 36]). The CV model is not based on the gradient of the image for the stopping process so that it can detect contours both

with and without gradients. The CV active contour model uses the energy minimization functional given by:

$$\min_{c_1,c_2\Gamma} F\left(\Gamma, c_1, c_2\right) = \min_{c_1,c_2\Gamma}\left\{\mu \text{length}(\Gamma) + \lambda_1 \int_{\text{inside}(\Gamma)} \left|u_0(x,y) - c_1\right|^2 dxdy + \lambda_2 \int_{\text{outside}(\Gamma)} \left|u_0(x,y) - c_2\right|^2 dxdy\right\} \quad (1)$$

where c_1 and c_2 are the average values of $u_0(x, y)$ inside and outside of the variable contour Γ, also μ, λ_1 and λ_2 are non-negative fixed parameters. The CV model [9] is non-convex but it can be converted into an equivalent and convex one [6].

Both categories of segmentation models mentioned above are for global segmentation due to the fact that all features are to be segmented. On the other hand, in many segmentation problems, we need to segment a particular aimed target object in the image and not all objects in it. This is a task of selective segmentation in which an object of interest is detected, given some additional information of geometric constraints. There are two ways to define geometric constraints. This paper follows the first way of defining geometric constraints in Gout-Guyader-Vese [15, 16, 18] who proposed an edge based method for selective segmentation. This work was improved by a mixed edge-based and region-based model by Badshah-Chen [4]. Other methods such as random walks [17], geodesics [5] and graph cut [30] use the distributions probability, edge based function or graph cut theory respectively. Those models are effective in some cases and can produce spurious objects (i.e. fail the selection) in some hard cases where the objects are near or the intensity difference is small, as shown by the example given in Fig. 1, where the intensity difference of triangle and rectangle is small.

The second way of defining geometric constraints can be found in [2] where geometric points outside as well as inside an intended objects are given. In addition, to speed up convergence, they make use of the Split Bregman method [14]. Although this paper focuses on the first way of defining geometric constraints, later, we shall compare our work with [2].

To improve the robustness of [4], in the recent work [29], we introduced a dual level set by equipping it with two level sets, one capturing all the boundaries (global level set) and a level set which evolves in the global level set which keeps the boundaries on the aimed target object. To help the local level set a new fidelity term that better splits the global domain was used. The

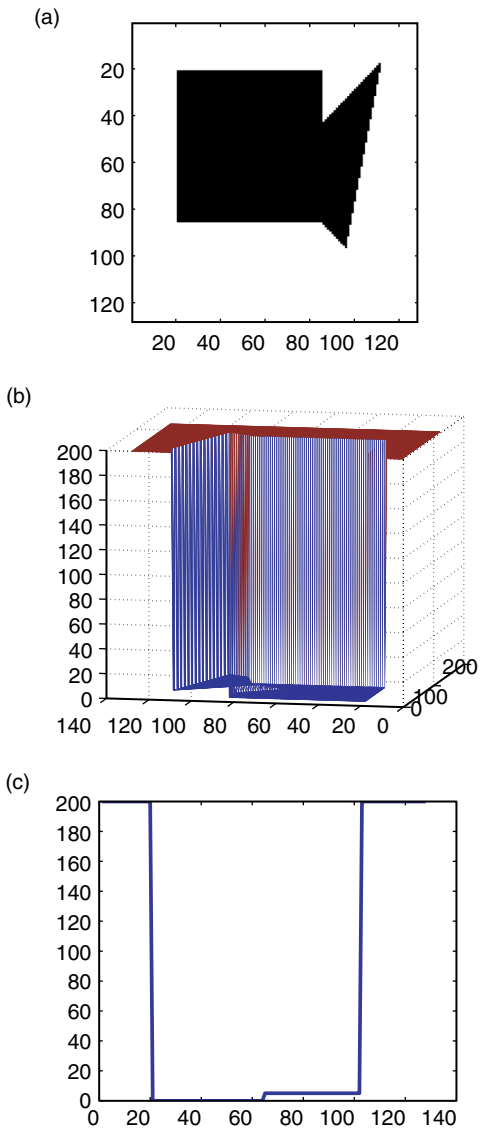

Figure 1. (a) A 2D composite image of a triangle over a rectangle; (b) Intensities of the image; (c) Vertical plane cut view through the middle of the image.

model is a combination of edge detection, markers distance function and active contour without edges. It has been shown that the model improves on old models, and is more reliable for harder problems (such as the example given in Fig. 1) where other models fail.

Although the Rada-Chen model [29] is reliable, its implementation is much slower than before because the complexity is doubled from replacing the previously single level set function by two level set functions. The natural question arisen here is the following: how can we design a model which uses only a single level set function and yet the reliability of selection is achieved? To this end, this paper introduces a new method based on one level set function, ensuring same or better performance compared with [2], and gives the same result as our previous presented dual level set method [29]. The new method is based optionally on the distance function from the given geometrical points and can be used only if needed when it is feasible to give an accurate estimate of the object of interest. The initial position of points for the proposed model has to place them near the boundaries of the target object. Our recommendation is to be placed inside the object so that we avoid any wrong initialization of the level set. An adaptive parameter edge detection function will be employed to better influence and decrease the functional as soon as we are in the boundaries and a crucial new area-based minimization fitting term is considered to enhance the model's reliability. Such an area fitting serves as a constraint rather than precise area preserving. In cases we have a trained datum for the object of interest the model might be transformed to a shape prior based segmentation, similar to Cremers-Sochen-Schnörr [12] or in case of occlusions similar to Thiruvenkadam-Chan-Hong [34]. This has not been concerned in this paper and will be in our future work.

This paper is organized in the following way. Section 2 contains a review of the Badshah-Chen model [4] and dual level-set model [29]. In Section 3 we present our proposed new model of minimization and derive the Euler-Lagrange equations. In Section 4 we describe the discretization of the method and develop an additive operator splitting (AOS) algorithm for solving the PDE, which is very efficient for this kind of problem. In Section 5 we give some experimental results. Examples of application of the method to different data-sets are presented. The new segmentation algorithm is compared to Badshah-Chen [4] and the dual level set [29]. Conclusions are given in Section 6.

2. REVIEW OF EXISTING VARIATIONAL SELECTIVE SEGMENTATION MODELS

As discussed, there exist many variational segmentation models in the literature on global segmentation and few models on selective segmentation. For the latter, we will review two segmentation models below that are directly related to this work.

2.1. Badshah-Chen model [4]

Below we start by reviewing the selective model by Badshah-Chen [4] which combines the edge based model of Gout-Guyader-Vese [16, 18] with region based information. For a given image $u_0(x, y)$, defined on the rectangular domain Ω, the selective segmentation idea can be described as the detection of image features that are defined in a closed domain to the geometrical points in a set $\mathcal{A} = \{w_i^* = (x_i^*, y_i^*) \in \Omega,\ 1 \leq i \leq n_1\} \subset \Omega$, consisting of n_1 distinct points near boundary of the object to be detected [4, 16], shown in Fig. 2. The aim in selective segmentation is to find an optimal contour $\Gamma_L \subset \Omega$ near the set $\mathcal{A}$, which in contrast with the global contour ($\Gamma_G = \partial\Omega$), represents a object which has minimal geometric distance from the set $\mathcal{A}$. Using the notation Γ instead of Γ_L, the Badshah-Chen [4] minimization equation is:

$$\min_{\Gamma,c_1,c_2} F\left(\Gamma, c_1, c_2\right) = \min_{\Gamma,c_1,c_2} \left\{ \mu \int_{\Gamma} d(x,y) g\left(\left|\nabla u_0(x,y)\right|\right) ds \right.$$
$$\left. + \lambda_1 \int_{\text{inside}(\Gamma)} \left|u_0(x,y) - c_1\right|^2 dxdy + \lambda_2 \int_{\text{outside}(\Gamma)} \left|u_0(x,y) - c_2{}^2 dxdy\right| \right\}. \tag{2}$$

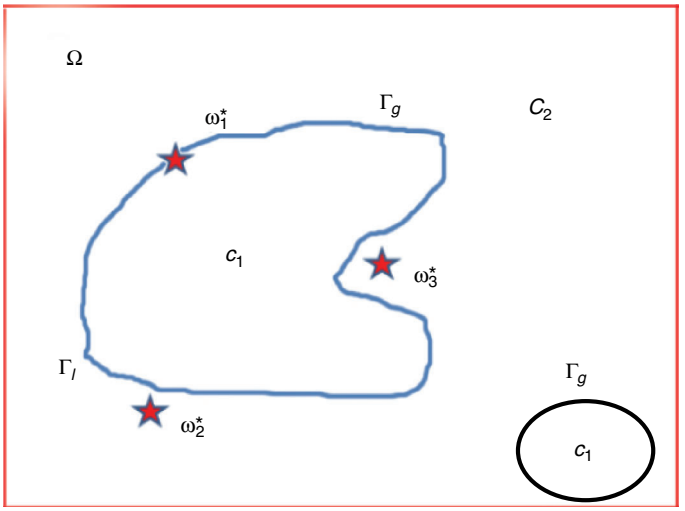

Figure 2. Graphical representation of the selective segmentation model. 3_L is the desired contour of the target object, w_i^* are the given markers of the object to be segmented, c_1 and c_2 are the mean intensities of the foreground and background respectively.

The first term is similar to the old Gut-Guyader-Vese model [16, 18], which is a geodesic active contour model [7] with the geometrical constraints being close to $\mathcal{A}$, while the second and third term bring an implementation of the region terms. In this model $g\left(\left|\nabla u_0(x,y)\right|\right) = \dfrac{1}{1+\left|\nabla u_0(x,y)\right|^2}$ is an edge detector function which helps to stop the evolving curve on the edges of the objects in an image. Clearly the $g(|\nabla u_0(x,\ y)|)$ function is almost 0 on edges where $|\nabla u_0(x,\ y)|$ is large and 1 in flat regions where $|\nabla u_0(x,\ y)|$ is small. The $d(x,\ y)$ function is a distance function, which will be required to stop the evolving curve when approaching the points from set $\mathcal{A}$. The function d is defined in the following way [18]:

$$d(x,y) = \text{distance}\left((x,y),\ \mathcal{A}\right) = \prod_{i=1}^{n_1}\left(1 - e^{-\frac{\left(x-x_i^*\right)^2}{2\tau^2}} e^{-\frac{\left(y-y_i^*\right)^2}{2\tau^2}}\right), \tag{3}$$

$\forall\,(x,\ y) \in \Omega$. Clearly the function d acts *locally* and will be approximately 0 in the neighborhood of points of $\mathcal{A}$. Other options for d can be chosen [29]. The aim is to find a contour Γ such that $d \simeq 0$ or $g \simeq 0$ along it. The contour Γ will stop at local minima where $d \simeq 0$ (in the neighborhood of points for *A*) or $g \simeq 0$ (near object boundaries).

Introducing the level set functions $\phi(x,\ y)$ defined such that

$$\begin{cases} \Gamma = \left\{\left(x,y\right) \in \Omega \middle| \phi\left(x,y\right) = 0\right\}, & \text{inside}(\Gamma) = \left\{\left(x,y\right) \in \Omega \;\middle|\; \phi\left(x,y\right) > 0\right\}, \\ & \text{outside}(\Gamma) = \left\{\left(x,y\right) \in \Omega \;\middle|\; \phi\left(x,y\right) < 0\right\}, \end{cases}$$

the functional (2) becomes:

$$\begin{aligned} \min_{\phi(x,y),c_1,c_2} F(\phi(x,y),c_1,c_2) = \mu\int_\Omega d(x,y)g(\left|\nabla u_0(x,y)\right|)\left|\nabla H(\phi(x,y))\right|dxdy \\ +\lambda_1\int_\Omega \left|u_0(x,y)-c_1\right|^2 H(\phi(x,y))dxdy \\ +\lambda_2\int_\Omega \left|u_0(x,y)-c_2\right|^2 (1-H(\phi(x,y)))dxdy, \end{aligned} \tag{4}$$

where *H* is the Heaviside function.

Since the Heaviside function is not differentiable at the origin, they consider the regularized version of H denoted by H_ϵ and the corresponding $d = H'$ by δ_ϵ. Different regularized Heaviside functions can be used [9, 41], e.g the following functions:

$$H_{1\epsilon} = \begin{cases} 0 & z < -\epsilon \\ \frac{1}{2}\left[1 + \frac{z}{\epsilon} + \frac{1}{\pi}\sin\left(\frac{\pi z}{\epsilon}\right)\right], & |z| \le \epsilon, \\ 1, & z > \epsilon, \end{cases}$$

$$H_{2\epsilon} = \frac{1}{2}\left(1 + \operatorname{erf}\left(\frac{\epsilon}{z}\right)\right), \qquad H_{3\epsilon} = \frac{1}{2}\left(1 + \frac{2}{\pi}\arctan\left(\frac{z}{\epsilon}\right)\right).$$

where $er\ f(x) = \frac{2}{\sqrt{\pi}}\int_0^x e^{-t^2}dt$ is error function, twice the integral of the Gaussian distribution with 0 mean and variance of $\frac{1}{2}$. Through a behavior analysis in [29] suggests that $H_{1\epsilon}$, or $H_{2\epsilon}$ are more suitable due to the small support in $[-\epsilon, \epsilon]$ and $H_{3\epsilon}$ may not be suitable for the extreme case where the feature of interest is less than 2 pixels away from other features; adjusting ϵ will resolve the problem. The minimization problem (4) in terms of the regularized version of H is:

$$\begin{aligned} \min_{\phi(x,y),c_1,c_2} F_\epsilon(\phi(x,y),c_1,c_2) = {} & \mu\int_\Omega W\delta_\epsilon(\phi(x,y))\left|\nabla\phi(x,y)\right| dxdy \\ & + \lambda_1\int_\Omega \left|u_0(x,y) - c_1\right|^2 H_\epsilon(\phi(x,y))dxdy \\ & + \lambda_2\int_\Omega \left|u_0(x,y) - c_2\right|^2 (1 - H_\epsilon(\phi(x,y)))dxdy, \end{aligned} \tag{5}$$

where $W = d(x, y)g\ (|\nabla z(x, y)|)$. Keeping ϕ fixed and minimizing with re- spect to c_1 and c_2, one gets the following for computing c_1 and c_2

$$c_1(\phi(x,y)) = \frac{\int_\Omega u_0(x,y)H_\epsilon(\phi(x,y))dxdy}{\int_\Omega H_\epsilon(\phi(x,y))dxdy} \tag{6}$$

$$c_2(\phi(x,y)) = \frac{\int_\Omega u_0(x,y)(1-H_\epsilon(\phi(x,y)))dxdy}{\int_\Omega (1-H_\epsilon(\phi(x,y)))dxdy} \tag{7}$$

if $\int_\Omega(1 - H_\epsilon(\phi(x, y)))dxdy > 0$ and $\int_\Omega H_\epsilon(\phi(x, y)))dxdy > 0$ (i.e if the curve has a nonempty interior and exterior in Ω). Finally keeping c_1 and c_2 fixed, one can minimize (5) with respect to $\phi(x, y)$. Thus we have the following Euler-Lagrange equation for ϕ

$$\delta_\epsilon(\phi)\mu\nabla\cdot\left(W\frac{\nabla\phi}{\left|\nabla\phi\right|}\right) - \delta_\epsilon(\phi)(\lambda_1(u_0(x,y)-c_1)^2 - \lambda_2(u_0(x,y)-c_2)^2) = 0,$$

in Ω, with $W\dfrac{\delta\epsilon(\phi)}{\left|\nabla\phi\right|}\dfrac{\partial\phi}{\partial\vec{n}}\Big|_{\partial\Omega} = 0.$

2.2. Dual Level-set Selective Segmentation Model [29]

The dual level-set selective segmentation model is based on the construction of two level-sets, respectively global and local level-sets, which essentially carry out a global segmentation and local selective segmentation. In this model new region-based terms are required and employed for the local level- sets. Denote by $\Gamma_G = \partial\Omega_G$ in Ω the global curve for locating of the features of the image u_0 and the desired selective curve by $\Gamma_L = \partial\Omega_L$ in Ω, where naturally assume Ω_L is contained in Ω_G, we have:

$$\begin{aligned}
&\min_{\Gamma_L,\Gamma_G,c_1,c_2} F\left(\Gamma_L,\Gamma_G,c_1,c_2\right)\\
&= \mu_1\int_{\Gamma_L} d(x,y)g\left(\left|\nabla u_0(x,y)\right|\right)ds + \mu_2\int_{\Gamma_G} g\left(\left|\nabla u_0(x,y)\right|\right)ds\\
&\quad + \lambda_{1G}\int_{\text{inside}(\Gamma_G)}\left|u_0(x,y)-c_1\right|^2 dxdy\\
&\quad + \lambda_{2G}\int_{\text{outside}(\Gamma_G)}\left|u_0(x,y)-c_2\right|^2 dxdy\\
&\quad + \lambda_1\int_{\text{inside}(\Gamma_L)}\left|u_0(x,y)-c_1\right|^2 dxdy\\
&\quad + \lambda_2\int_{\text{outside}(\Gamma_L)\cap\text{inside}(\Gamma_G)}\left|u_0(x,y)-c_1\right|^2 dxdy\\
&\quad + \lambda_3\int_{\text{outside}(\Gamma_L)\cap\text{outside}(\Gamma_G)}\left|u_0(x,y)-c_2\right|^2 dxdy,
\end{aligned} \tag{8}$$

where $g(|\nabla u_0(x,\ y)|)$ and $d(x,\ y)$ are defined as in [4] and the parameters μ_1, μ_2, λ_{1G}, λ_{2G}, λ_1, λ_2, λ_3 are all positive. To penalize the level set function to a signed distance function a new term similar to [22] idea is used. Adding the term $P\left(\phi\right)=\frac{1}{2}\int_{\Omega}\left(\left|\nabla\phi\right|-1\right)^2 dxdy$ we avoid re-initialization so, with $W=\ dg(|\nabla u_0|)$, (8) is written as

$$\begin{aligned}
&\min_{\phi_L(x,y),\,\phi_G(x,y),c_1,c_2} F_\epsilon\left(\phi_L(x,y),\phi_G(x,y),c_1,c_2\right)\\
&=\ \mu_1\int_\Omega W\delta_\varepsilon(\phi_L(x,y))\left|\nabla\phi_L(x,y)\right|H_\epsilon(\phi_G(x,y))dxdy\\
&\quad+\frac{\mu_L}{2}\int_\Omega\left(\left|\nabla\phi_L(x,y)\right|-1\right)^2 dxdy\\
&\quad+\mu_2\int_\Omega g\left(\left|\nabla u_0(x,y)\right|\right)\delta_\epsilon\left(\phi_G(x,y)\right)\left|\nabla\phi_G(x,y)\right|dxdy\\
&\quad+\frac{\mu_{\mathrm{G}}}{2}\int_\Omega\left(\left|\nabla\phi_G(x,y)\right|-1\right)^2 dxdy\\
&\quad+\lambda_{1\mathrm{G}}\int_\Omega\left|u_0(x,y)-c_1\right|^2 H_\epsilon\left(\phi_G\left(x,y\right)\right.dxdy\\
&\quad+\lambda_{2\mathrm{G}}\int_\Omega\left|u_0(x,y)-c_2\right|^2\left(1-H_\epsilon\left(\phi_G\left(x,y\right)\right)\right.dxdy\\
&\quad+\lambda_1\int_\Omega\left|u_0(x,y)-c_1\right|^2 H_\epsilon\left(\phi_L\left(x,y\right)\right.dxdy\\
&\quad+\lambda_2\int_\Omega\left|u_0(x,y)-c_1\right|^2\left(1-H_\epsilon\left(\phi_L\left(x,y\right)\right)\right)H\left(\phi_G\left(x,y\right)\right.dxdy\\
&\quad+\lambda_3\int_\Omega\left|u_0(x,y)-c_2\right|^2\left(1-H_\epsilon\left(\phi_L\left(x,y\right)\right)\right)\left(1-H_\epsilon\left(\phi_G\left(x,y\right)\right)\right)dxdy.
\end{aligned}\tag{9}$$

Here μ_L, μ_G are positive. Keeping ϕ fixed and minimizing with respect to c_1 and c_2, we compute c_1 and c_2 as follows (letting $T=1-H_\epsilon(\phi_L)$):

$$c_1=\frac{\lambda_{1\mathrm{G}}\int_\Omega u_0 H_\varepsilon\left(\phi_G\right)dxdy+\lambda_1\int_\Omega u_0 H_\epsilon\left(\phi_L\right)dxdy+\lambda_2\int_\Omega u_0 T H_\epsilon\left(\phi_G\right)dxdy}{\lambda_{1\mathrm{G}}\int_\Omega H_\varepsilon\left(\phi_G\right)dxdy+\lambda_1\int_\Omega H_\epsilon\left(\phi_L\right)dxdy+\lambda_2\int_\Omega T H_\epsilon\left(\phi_G\right)dxdy},\tag{10}$$

$$c_2=\frac{\lambda_{2\mathrm{G}}\int_\Omega u_0\left(1-H_\epsilon\left(\phi_G\right)\right)dxdy+\lambda_3\int_\Omega u_0 T\left(1-H_\epsilon\left(\phi_G\right)\right)dxdy}{\lambda_{2\mathrm{G}}\int_\Omega\left(1-H_\epsilon\left(\phi_G\right)\right)dxdy+\lambda_3\int_\Omega T\left(1-H_\epsilon\left(\phi_G\right)\right)dxdy}\tag{11}$$

if we assume the $\phi_G(x, y)$ has neither empty interior nor empty exterior.

Keeping c_1 and c_2 fixed and minimizing (9) with respect to $\phi_L(x, y)$ and $\phi_G(x, y)$ the following Euler-Lagrange equation can be derived:

$$\begin{cases} \mu_1\delta_\epsilon\left(\phi_L\right)\nabla\cdot\left(WH_\epsilon\left(\phi_G\right)\dfrac{\nabla\phi_L}{\left|\nabla\phi_L\right|}\right)+\mu_L\nabla\cdot\left(\left(1-\dfrac{1}{\left|\nabla\phi_L\right|}\right)\nabla\phi_L\right) \\ +\delta_\epsilon\left(\phi_L\right)\left(-\lambda_1\left(u_0\left(x,y\right)-c_1\right)^2+\lambda_2\left(u_0\left(x,y\right)-c_1\right)^2 H_\epsilon\left(\phi_G\right)\right. \\ \left.+\lambda_3\left(u_0\left(x,y\right)-c_2\right)^2\left(1-H_\varepsilon\left(\phi_G\right)\right)\right)=0 \quad \text{in } \Omega \end{cases}$$

and

$$\begin{cases} \mu_2\delta_\epsilon\left(\phi_G\right)\nabla\cdot\left(g\left(x,y\right)\dfrac{\nabla\phi_G}{\left|\nabla\phi_G\right|}\right)+\mu_G\nabla\cdot\left(\left(1-\dfrac{1}{\left|\nabla\phi_G\right|}\right)\nabla\phi_G\right) \\ +\delta_\epsilon\left(\phi_G\right)\left(-\mu_1 W\left(x,y\right)\left|\nabla H_\epsilon\left(\phi_L\right)\right|\right. \\ +\delta_\epsilon\left(\phi_G\right)\left(-\lambda_{1G}\left(u_0\left(x,y\right)-c_1\right)^2+\lambda_{2G}\left(u_0\left(x,y\right)-c_2\right)^2-\lambda_2\left(u_0\left(x,y\right)-c_1\right)^2 T\right. \\ \left.\left.+\lambda_3\left(u_0\left(x,y\right)-c_2\right)^2 T\right)=0 \text{ in } \Omega, \end{cases}$$

where $\left.\dfrac{\partial\phi_L}{\partial\vec{n}}\right|_{\partial\Omega}=\left.\dfrac{\partial\phi_G}{\partial\vec{n}}\right|_{\partial\Omega}=0.$

The equations for ϕ_L and ϕ_G will be iteratively updated. The model showed good accuracy in hard problems but slow convergence due to updating two level-sets rather than one.

3. A NEW ONE LEVEL SELECTIVE SEGMENTATION MODEL

In this section we propose a novel one level selective segmentation variational model, using the key idea of area fitting. For a given image $u_0(x, y)$, defined on the rectangular domain Ω, our aim is to detect an image feature/object that is close to the geometrical domain of the points $\mathcal{A}=\{w_i^*=(x_i^*,y_i^*)\in\Omega,\ 1\le i\le n_1\}\subset\Omega$,

which are placed inside the object or in the boundaries, and at the same time are an indicator of where our initialization for the level set has to be placed. The given points can be at the same time an indicator of the relative size of the object in the area term so, if we consider the polygon area constricted with the given points, we can get an approximate ratio of the object in comparison with the whole domain Ω. On the other hand, the mean intensity of this polygon is approximately the intensity of the target object, which we will denote by c_1 in what follows.

Since the distance function gives a local weight in a small neighborhood on given markers, to have a good influence from this function we need to increase the number of points in the set $\mathcal{A}$ and for more they have to be near the boundaries, which is not practically convenient. For this reason we want the program to be less dependent of the distance function and only needed when it is feasible to give an accurate estimate of the object of interest. In this way we do not fail in cases where inaccurate geometrical information is given. We start by constructing the energy minimization functional:

$$\begin{aligned}\min_{\Gamma, c_2} F\left(\Gamma, c_2\right) = \min_{\Gamma, c_2} \Bigg\{ & \mu \int_{\Gamma} g\left(\left|\nabla u_0\left(x,y\right)\right|\right) dxdy \\ & + \lambda_1 \int_{\text{inside}(\Gamma)} \left|u_0\left(x,y\right) - c_1\right|^2 dxdy \\ & + \lambda_2 \int_{\text{outside}(\Gamma)} \left|u_0\left(x,y\right) - c_2\right|^2 dxdy \\ & + \nu \left\{ \left(\int_{\text{inside}(\Gamma)} dxdy - A_1 \right)^2 + \left(\int_{\text{outsite}(\Gamma)} dxdy - A_2 \right)^2 \right\}, \end{aligned} \tag{12}$$

where λ_1, λ_2, μ, ν and are empirical weights, g is the edge detector function applied to the original image, c_1 is the known mean of the polygon constructed with the given markers (with the supposition that the markers are placed inside the object or not too far the boundaries), c_2 is a region term defined below in equation (16) representing the mean intensity outside the target object. We remark that in region growing methods c_1 would be the intensity of a given pixel (i.e. unreliable due to noise or non-homogeneity) but our mean is a more reliable quantity; moreover we also have the option of updating c_1. The function g is an adaptive parameter edge detection function given by:

$$g\left(\left|\nabla u_0\left(x,y\right)\right|\right) = \frac{1}{1 + k\left|\nabla u_0\left(x,y\right)\right|^2}, \tag{13}$$

with k a positive constant. The constant k is used to help to sharpen the edges especially when the intensity difference is small, since in this case we know that near the edges $|\nabla u_0(x, y)|$ might be not big enough that the function $g(|\nabla u_0(x, y)|)$ is approximately 0. In case of strong noise a smooth version of $u_0(x, y)$ can be used, e.g $G_\sigma(x, y) * u_0(x, y)$, a Gaussian convolution with $G_\sigma(x, y) = \sigma^{-1/2} e^{-|x^2 + y^2|/4\sigma}$, which helps to eliminate the height of non-desired frequencies.

Analyzing the energy above we can notice that the first term (weighted by μ) is the regularizer of the inverse problem and expresses the weighted geodesic length of the contour. The second and the third term (weighted by λ_1, λ_2) are region fitting terms to the mean intensity inside the object and outside it respectively. The forth and fifth term (weighted by ν) are a priori terms stating that the volume area of each object remains close to a reference area (or volume for 3-D) A_i, $i = 1, 2$. In our case we compute A_i as an area of the polygon inside and outside the given markers. In this way we have an approximation of the area of the object we are looking to capture. Rewriting the above equation in terms of the level-set we have:

$$\begin{aligned}\min_{\phi(x,y),\, c_2} F\left(\phi\left(x,y\right), c_2\right) = {} & \mu \int_\Omega g\left(\left|\nabla u_0\left(x,y\right)\right|\right)\left|\nabla H\left(\phi\left(x,y\right)\right)\right| dxdy \\ & + \lambda_1 \int_\Omega \left|u_0\left(x,y\right) - c_1\right|^2 H\left(\phi\left(x,y\right)\right) dxdy \\ & + \lambda_2 \int_\Omega \left|u_0\left(x,y\right) - c_2\right|^2 \left(1 - H\left(\phi\left(x,y\right)\right)\right) dxdy \\ & + \nu \left\{\left(\int_\Omega H\left(\phi\left(x,y\right)\right) dxdy - A_1\right)^2 \right. \\ & \left. + \left(\int_\Omega \left(1 - H\left(\phi\left(x,y\right)\right) dxdy\right) - A_2\right)^2 \right\} dxdy.\end{aligned} \tag{14}$$

The non-differentiable H function can be replaced by H_ϵ a regularized Heaviside function as in [3, 9] and we get:

$$\begin{aligned}\min_{\phi(x,y),\, c_2} F_\epsilon\left(\phi\left(x,y\right), c_2\right) = {} & \mu \int_\Omega g\left(\left|\nabla u_0\left(x,y\right)\right|\right) \delta_\epsilon\left(\phi\left(x,y\right)\right)\left|\nabla\left(\phi\left(x,y\right)\right)\right| \\ & + dxdy + \lambda_1 \int_\Omega \left|u_0\left(x,y\right) - c_1\right|^2 H_\epsilon\left(\phi\left(x,y\right)\right) dxdy \\ & + \lambda_2 \int_\Omega \left|u_0\left(x,y\right) - c_2\right|^2 \left(1 - H_\epsilon\left(\phi\left(x,y\right)\right)\right) dxdy \\ & + \nu \left\{\left(\int_\Omega H_\epsilon\left(\phi\left(x,y\right)\right) dxdy - A_1\right)^2 \right. \\ & \left. + \left(\int_\Omega \left(1 - H_\epsilon\left(\phi\left(x,y\right)\right) dxdy\right) - A_2\right)^2 \right\} dxdy,\end{aligned} \tag{15}$$

where $\delta_\epsilon(\phi(x,\ y)$ is a regularized Delta function corresponding to the Heaviside function introduced above. Keeping $\phi(x,\ y)$ fixed and minimizing with respect to the unknown intensity outside the object, one gets the following equations for computing c_2:

$$c_2\left(\phi\left(x,y\right)\right)=\frac{\int_\Omega u_0\left(x,y\right)\left(1-H_\epsilon\left(\phi\left(x,y\right)\right)\right)dxdy}{\int_\Omega\left(1-H_\epsilon\left(\phi\left(x,y\right)\right)\right)dxdy} \tag{16}$$

if $\int_\Omega (1–H_\epsilon(\phi(x,\ y)))dxdy > 0$ (i.e if the curve is nonempty in Ω). We have to mention that c_1 can be considered as an unknown and minimized with respect to it to obtain $c_1\left(\phi(x,y)\right)=\frac{\int_\Omega u_0(x,y)H_\epsilon\left(\phi(x,y)\right)dxdy}{\int_\Omega H_\epsilon\left(\phi(x,y)\right)dxdy}$ in the case of wrong markers placed outside the object.

Keeping c_1 and c_2 fixed and denoting $W = g(|\nabla u_0|)$, we minimize (15) with respect to $\phi(x,\ y)$ and get the following Euler-Lagrange equation:

$$\begin{aligned}\delta_\epsilon\left(\phi\right)\Bigg\{\mu\nabla\cdot\left(W\frac{\nabla\phi}{\left|\nabla\phi\right|}\right)-\left[\lambda_1\left(u_0\left(x,y\right)-c_1\right)^2-\lambda_2\left(u_0\left(x,y\right)-c_2\right)^2\right]\\ -\ \nu\left[\left(\int_\Omega H\ dxdy-A_1\right)-\left(\int_\Omega\left(1-H\right)dxdy-A_2\right)\right]\Bigg\}=0\ \ \text{in}\ \Omega,\end{aligned} \tag{17}$$

where $\left.\frac{\partial\phi}{\partial\vec{n}}\right|_{\partial\Omega}=0.$ Derivation of the Euler-Lagrange equation is given in the Appendix.

In case the markers are near the boundaries $W = g(|\nabla u_0(x,\ y)|)|$ can be replaced by $W = d(x,y)g(|\nabla u_0(x,y)|)|$, similar to Badshah-Chen or Gout-Guyader [4, 18]. In equation (17) balloon terms such as $\alpha W|\nabla\phi|$ can be added to speed up the convergence. The final equations of ϕ can be written in the form:

$$\begin{aligned}\delta_\epsilon\left(\phi\right)\Bigg\{\mu\nabla\cdot\left(W\frac{\nabla\phi}{\left|\nabla\phi\right|}\right)-\left[\lambda_1\left(u_0\left(x,y\right)-c_1\right)^2-\lambda_2\left(u_0\left(x,y\right)-c_2\right)^2\right]\\ -\ \nu\left[\left(\int_\Omega Hdxdy-A_1\right)-\left(\int_\Omega\left(1-H\right)dxdy-A_2\right)\right]\Bigg\}-\ \alpha W\left|\nabla\phi\right|=0.\end{aligned} \tag{18}$$

To avoid re-initialization of the level set function $\phi(x,\ y)$, a term can be added in (18) such that the level set can be automatically scaled. To penalize the level set function from a signed distance function with new term similar to the Li-Xu-Gui-Fox idea [22] can be used avoiding re-initialization $P(\phi) = \theta \int_{\Omega} \frac{1}{2}\left(\left|\nabla\phi\right| - 1\right)^2 dxdy$. After derivation this term will have the form

$$\theta\nabla \cdot \left(\left(1 - \frac{1}{\left|\nabla\phi\right|}\right)\nabla\phi\right).$$

For more about re-initialization techniques you can refer to [22, 27]. In our experiments re-initialization was not required.

The approximation of equation (18) can be done by introducing an artificial time step t and getting the gradient descent method. In this way we get the following evolution equation:

$$\begin{aligned}\frac{\partial\phi}{\partial t} = \delta_{\epsilon}\left(\phi\right)\Bigg\{\mu\nabla\cdot\left(W\frac{\nabla\phi}{\left|\nabla\phi\right|}\right) - \left[\lambda_1\left(u_0(x,y) - c_1\right)^2 - \lambda_2\left(u_0(x,y) - c_2\right)^2\right] \\ - \nu\left[\left(\int_{\Omega} H dxdy - A_1\right) - \left(\int_{\Omega}\left(1 - H\right)dxdy - A_2\right)\right]\Bigg\} - \alpha W\left|\nabla\phi\right| = 0,\end{aligned} \tag{19}$$

with Neumann boundary conditions.

4. AN ADDITIVE OPERATOR SPLITTING ALGORITHM

In order to solving equation (19), a fast and a low computational cost method is required. The additive operator splitting (AOS) method, proposed by Tai *et al*. [23] and Weickert [39] is widely applied to a diffusion equation, see [4, 18, 38]. This method allows the decomposition of the two-dimensional problem into two one-dimensional ones. To implement this algorithm in our method we have to make the discretization of the equation (19), form a semi-implicit linear system and develop the iterative approximation scheme which solves a diagonally dominant tridiagonal linear system.

We first recall the evolution equation satisfied by:

$$\begin{aligned}\frac{\partial\phi}{\partial t} &= \mu\delta_{\epsilon}(\phi)\nabla\cdot\left(W\frac{\nabla\phi}{\left|\nabla\phi\right|}\right)-\alpha W(x,y)\left|\nabla\phi\right| \\ &+\delta_{\epsilon}(\phi)\left\{-\left[\lambda_1(u_0(x,y)-c_1)^2-\lambda_2(u_0(x,y)-c_2)^2\right]\right. \\ &\left.-\nu\left[\left(\int_{\Omega}Hdxdy-A_1\right)-\left(\int_{\Omega}(1-H)dxdy-A_2\right)\right]\right\},\end{aligned} \tag{20}$$

where $\phi(x,\ y,\ 0)=\phi^0(x,\ y)$ and $\left.\frac{\partial\phi}{\partial\vec{n}}\right|_{\partial\Omega}=0.$ To avoid singularities we can replace the term $|\nabla\phi|$ with $\left|\nabla\phi\right|_{\beta}=\sqrt{\phi_x^2+\phi_y^2+\beta}$, for a small β. Denoting

$$\begin{aligned}f=\delta_{\epsilon}(\phi)&\left\{\begin{array}{l}-\left[\lambda_1(u_0(x,y)-c_1)^2-\lambda_2\left(u_0\left(x,y\right)-c_2\right)^2\right]- \\ \nu\left[\left(\int_{\Omega}Hdxdy-A_1\right)-\left(\int_{\Omega}\left(1-H\right)dxdy-A_2\right)\right]\end{array}\right\} \\ &-\alpha W(x,y)\left|\nabla\phi\right|,\end{aligned} \tag{21}$$

and $E=\frac{W}{\left|\nabla\phi\right|_{\beta}}$, equations (20) can be written in the compact form:

$$\begin{cases}\dfrac{\partial\phi}{\partial t}=\mu\delta_{\epsilon}(\phi)\nabla.(E\nabla\phi)+f \\ \qquad=\mu\delta_{\epsilon}(\phi)(\partial_x(E\partial_x\phi)+\partial_y(E\partial_y\phi))+f.\end{cases} \tag{22}$$

Discretizing in the spatial step, the equation (20) can be rewritten in the matrix-vector form:

$$\frac{\phi^{n+1}-\phi^n}{\Delta t}=\sum_{l=1}^{2}A_l(\phi^n)\phi^{n+1}+f(x,y)$$

where Δt is the time step size, n denotes the n^{th} iteration and A_l is the diffusion quantity in the l direction ($l=1$ and $l=2$ respectively for x and y direction for

the two dimensional case). We can rewrite the above equation in the semi-implicit form:

$$\phi^{n+1} = \left(I - \Delta t \sum_{l=1}^{2} A_l\left(\phi^n\right) \right)^{-1} \hat{\phi}^n \text{ for } l = 1,2 \text{ and } \hat{\phi}^n = \phi^n + \Delta t f(x,y)$$

which, by employing the AOS scheme, can be split additively as shown below to define the AOS solution

$$\phi^{n+1} = \frac{1}{2} \sum_{l=1}^{2} \left(I - 2\Delta t A_l\left(\phi^n\right) \right)^{-1} \hat{\phi}^n \tag{23}$$

Here the matrices A_1, for $l = 1, 2$, are tridiagonal matrices derived using finite differences:

$$\begin{aligned}
&\left(A_1\left(\phi^n\right)\phi^{n+1}\right)_{i,j} = \mu\delta_\epsilon(\phi^n)\left(\partial_x\left(E\partial_x\phi^{n+1}\right)\right)_{i,j} \\
&= \mu\delta_\epsilon(\phi^n)\frac{E^n_{i+1/2,j}\left(\partial_x\phi^{n+1}\right)_{i+1/2,j} - E^n_{i-1/2j}\left(\partial_x\phi^{n+1}\right)_{i-1/2,j}}{h_x} \\
&= \mu\delta_\epsilon(\phi^n)\frac{\dfrac{E^n_{i+1,j}+E^n_{i,j}}{2}\left(\dfrac{\phi^{n+1}_{i+1,j}-\phi^{n+1}_{i,j}}{h_x}\right) - \dfrac{E^n_{i,j}+E^n_{i-1,j}}{2}\left(\dfrac{\phi^{n+1}_{i,j}-\phi^{n+1}_{i-1,j}}{h_x}\right)}{h_x} \\
&= \mu\delta_\epsilon(\phi^n)\frac{E^n_{i+1,j}+E^n_{i,j}}{2h_x^2}\left(\phi^{n+1}_{i+1,j}-\phi^{n+1}_{i,j}\right) \\
&-\mu\delta_\epsilon(\phi^n)\frac{E^n_{i,j}+E^n_{i-1,j}}{2h_x^2}\left(\phi^{n+1}_{i,j}-\phi^{n+1}_{i-1,j}\right),
\end{aligned}$$

and similarly

$$\left(A_2\left(\phi^n\right)\phi^{n+1}\right)_{i,j} = \mu\delta_\epsilon(\phi^n)\left(\partial_y\left(E\partial_y\phi^{n+1}\right)\right)_{i,j}$$

$$= \mu\delta_\epsilon(\phi^n)\frac{E^n_{i,j+1/2}\left(\partial_y\phi^{n+1}\right)_{i,j+1/2} - E^n_{i,j-1/2}\left(\partial_y\phi^{n+1}\right)_{i,j-1/2}}{h_y}$$

$$= \mu\delta_\epsilon(\phi^n)\frac{\frac{E^n_{i,j+1}+E^n_{i,j}}{2}\left(\frac{\phi^{n+1}_{i,j+1}-\phi^{n+1}_{i,j}}{h_x}\right) - \frac{E^n_{i,j}+E^n_{i,j-1}}{2}\left(\frac{\phi^{n+1}_{i,j}-\phi^{n+1}_{i,j-1}}{h_y}\right)}{h_y}$$

$$= \mu\delta_\epsilon(\phi^n)\frac{E^n_{i,j+1}+E^n_{i,j}}{2h_y^2}\left(\phi^{n+1}_{i,j+1}-\phi^{n+1}_{i,j}\right)$$

$$-\mu\delta_\epsilon(\phi^n)\frac{E^n_{i,j}+E^n_{i,j-1}}{2h_y^2}\left(\phi^{n+1}_{i,j}-\phi^{n+1}_{i,j-1}\right).$$

Algorithm 1 AOS Method Algorithm for Solving the One Level Selective Method: $\phi^k \leftarrow OLSS(\phi^{(0)}, \mathcal{A}, \mu,\nu,\beta, \alpha, \epsilon, maxit, tol)$.

Calculate the edge based function and area of the polygon (distance function optional);

$n = 1$, Compute f from equation (21), $\phi^{(1)} = \phi^{(0)}$;

for $iter = 1 : maxit$ **do**

Compute $\phi^{(n)}$ using (23):

$$\phi_i^{(n+1)} \leftarrow \frac{1}{2}\sum_{l=1}^{2}\left(I - 2\Delta t A_l\left(\phi^n\right)\right)^{-1}\hat{\phi}^n$$

If $||\phi^{(n+1)} - \phi^{(n)}|| < tol$ or $iter > maxit$, set $\phi^{(k)} \leftarrow \phi^{(n-1)}$ Break; else $\phi^{(k)} \leftarrow \phi^{(n-1)}$

update f from equation (21)

end for

5. EXPERIMENTAL RESULTS

In order to illustrate the performance and the accuracy of the proposed method, experiments were carried out on synthetic, CT and MRI 2-D images. We like to emphasize that in all the results shown below for the new method the distance function was not considered, in other words $d(x, y) = 1$. Three kinds of experimental results are shown:

- demonstrating that our new segmentation method works better than the Badshah-Chen model [4] for segmenting hard cases, such as the objects

shown in Fig. 1;

- comparing with the Nguyen-Cai-Zhang-Zheng model [2] which is the state-of-the-arts method and is known for its robustness, accurate boundary with a small amount of user interaction. It should be noticed that our model performs better then Nguyen-Cai-Zhang-Zheng model in some cases where the objects have same intensity and the boundaries are vague or object with same intensity;
- comparing with the Rada-Chen model [29] which is known for good performance in selecting the right object in cases of low intensity difference or with objects which are close to each other.

In the following experiments the parameters Δt, λ_1, λ_2, α, h (step size), ϵ and β, have been fixed at $\Delta t = 0.1$, $\lambda_1 = \lambda_2 = 1$, $\alpha = -0.01$, $h = 1$, $\epsilon = 1$, and $\beta = 10^{-6}$, respectively. Differently sized images $n \times n = 128 \times 128$, 256×256 have been tested and show the same satisfactory results. To stop the program, the relative residual 10^{-2} has been used.

Through the experiments it was observed that the parameters μ, ν can be in a range between $\mu = 100$ to $n^2/10$ and $\nu = 0.1$ to 1 which gave similar result. Increasing of the parameter k gives better performance in hard cases. In hard cases we considered k greater than 100.

The first initial level set has been constricted as a sign distant function of the given polygon constructed with the markers. This initialization has been found as more proper in our experiments. The experimental results show that if the markers are outside the object but not inside nearby objects the method works, in contrast with the case where the markers are placed near the boundaries or inside other objects in which the method fails by capturing the nearby objects.

Since $H_{3\epsilon}$ has a bigger support in the interval $[-\epsilon, \epsilon]$, which means that with it a moderately large ϵ may lead to spurious results, in our experiments for the local level set, as approximations for the heaviside function we use $H_{1\epsilon}$ or $H_{2\epsilon}$ with $\epsilon = h = 1$, and for the global level set $H_{3\epsilon}$ with $\epsilon = h = 1$;.

5.1. Test Set 1 — Robustness and Accuracy of the New Model, and Comparison with Badsah-Chan Model

In the first test set, we demonstrate the ability of recognizing objects which have a small intensity difference. Fig. 1 shows a rectangle and triangle with a non empty intersection and with small intensity difference of those two objects. The Fig. 3 (c) and (d) presents the satisfactory experimental results using the new model algorithm for capturing both of these objects separately, while the

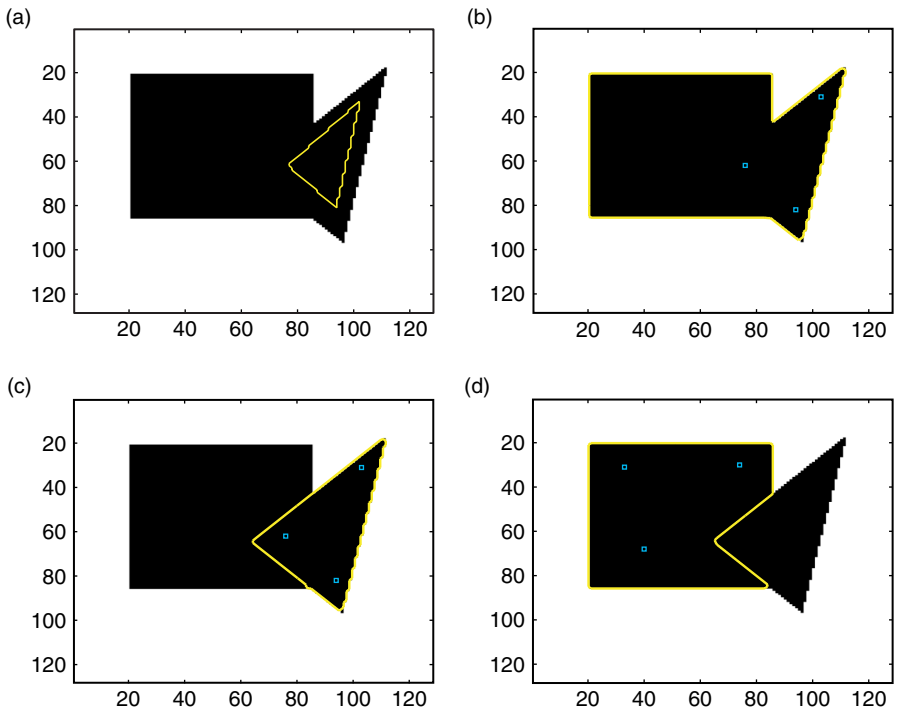

Figure 3. Test Set 1 – Comparison with Badshah-Chen model [4]: (a) First level set; (b) Unsuccessful result by [4] model for the case of two object with small intensity difference; (c-d) Successful result by new model for the case of two objects with small intensity difference.

old Badshah-Chan model would easily fail in this case, as shown in Fig. 3(b), where all black area was segmented. The real life image or the medical images are a real challenge for segmentation in general and especially for selective segmentation, due to poor quality and noise. In Fig. 4(c) and (d) we show that the model works satisfactorily with this kind of images. All these images have been shown as hard cases in the Rada-Chen [29] paper and segmented correctly by a dual level set, results which are the same with the one we already showed in Fig. 3 (c), (d), Fig. 4(c) and (d).

5.2. Test Set 2 — Comparison with Model [2]

For the test images in Fig. 3 and 4(c) and for almost all the images we present in this paper, we see that the Nguyen-Cai-Zhang-Zheng model [2] gives same

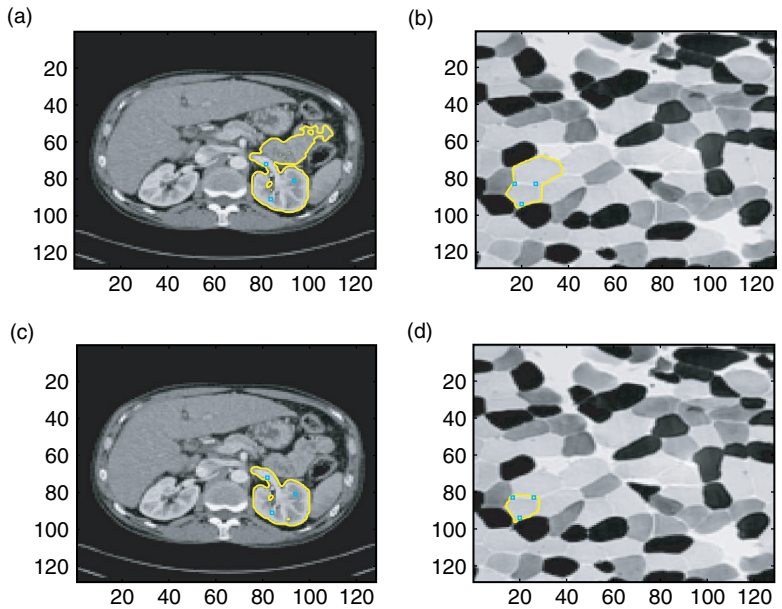

Figure 4. Test Set 1 – Comparison with the Badshah-Chen model [4]: (a) Unsuccessful result by [4] model for the case CT images where the organs are nearby, with small intensity difference and in presence of noise; (b) Unsuccessful result by [4] model for the case of a biological image where the cells are of the same intensity or with small intensity difference; (c) Successful results with the new model in case of CT images where the organs are nearby, with small intensity difference and in presence of noise; (d) Successful result by new model for the case of a biological image where the cells are of the same intensity or with small intensity difference.

satisfactory results as our model. For briefness we will not show too many results that both models give satisfactory results; Fig. 5 shows the successful segmentation of the kidney by Nguyen-Cai-Zhang-Zheng model in a CT image. This test set also includes a few examples where our model performs better than model [2]. Although the performance of Nguyen-Cai-Zhang-Zheng model [2] is much better than other methods such as [4], its results still contain some artifacts due to similar appearance. The method cannot handle transparent or semi-transparent boundaries; Fig. 6 gives a failure example, where our method is able to segment the target cell in a clean way while model [2] fails. Fig. 7 shows another example where model [2] fails while our model succeeds in Fig. 8(a).

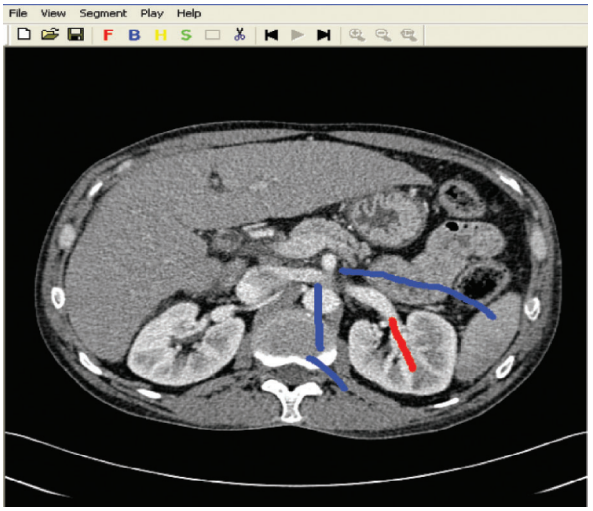

(a) Two types of strokes has been labeling some foreground and background pixels

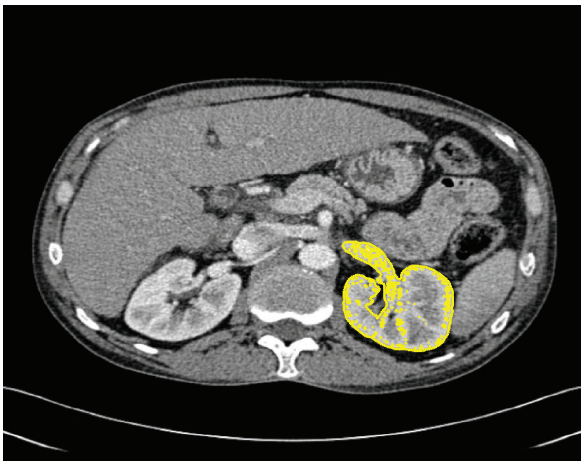

(b) Successful segmentation of the kidney by Nguyen-Cai-Zhang-Zheng model (2)

Figure 5. Test Set 2 – Comparison with Nguyen-Cai-Zhang-Zheng model [2]. Successful result by Nguyen-Cai-Zhang-Zheng model for the case of kidney segmentation in a CT image.

5.3. Test Set 3 — comparison with model [29]

We continue our experiments by giving more examples and compare our model with the DLSS method [29]. Here we show 12 more different images,

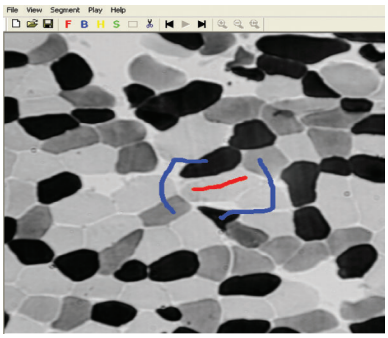

(a) Two types of strokes has been labeling some foreground and background pixels

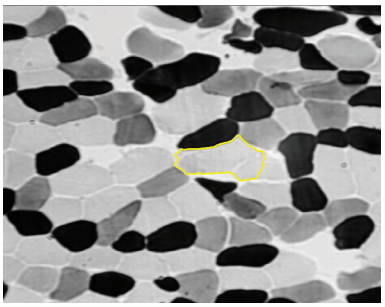

(b) Unsuccessful result of the cell by Nguyen-Cai-Zhang-Zheng model (2)

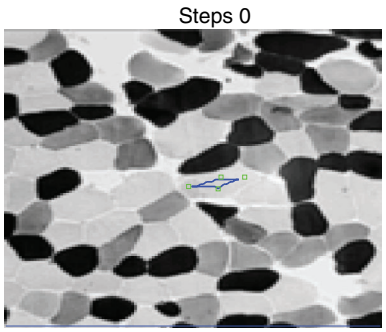

(c) In green are 4 given markers and in blue the first level set

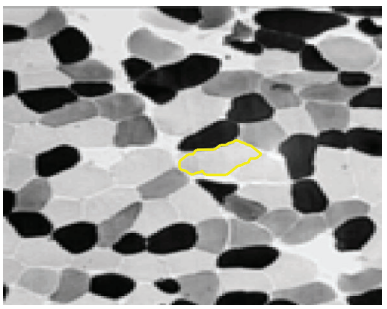

(d) Successful segmentation of the cell with the new model

Figure 6. Test Set 2 – Comparison with Nguyen-Cai-Zhang-Zheng model [2]. Successful result by new model for the case of two cells with same intensity and semi-transparent boundaries.

which can be found as successfully selected by the DLSS method [29]. All of the testing examples, as shown in Fig. 8, give satisfactory segmentation which is almost the same result as with the DLSS method, which for the sake of brevity we do not show. The first five images in Fig. 8, (a), (b), (c), (d), (e) respectively, are artificial images and from the results we conclude that the model works satisfactorily for cases where the features are nearby and with different shapes, while the last images, Fig. 8 (f), (g), (h), (i), (j), (k), (l), show an accurate segmentation of biological and medical images, which are considered as much more hard cases due to the low-quality data. Since in the case of the dual level sets two level set need to be updated the model

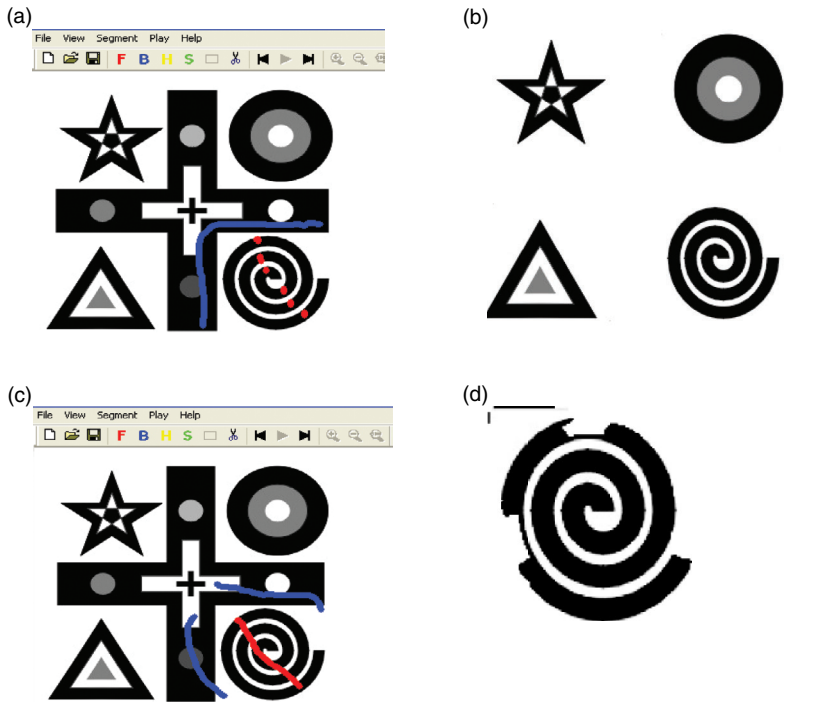

Figure 7. Test Set 2 – Unsuccessful result by Nguyen-Cai-Zhang-Zheng model [2] for the spiral object. The first column shows the given strokes for the foreground (in red) and background (in blue), while the second column shows the segmentation result with the Nguyen-Cai-Zhang-Zheng model [2]. Our new method shows successful result for this case as shown in Fig. 8(a).

suffers from slow convergence. Table 1 shows clearly this fact. In this table we compare in CPU time the new model with the old dual level set model [29], and find out that the new model is at least two or three times faster, result which was obtained in all the experiments we did without exceptions.

6. CONCLUSIONS

In this paper we presented a new variational selective segmentation model with one level set function which performs reliable segmentation, improving on two related models proposed recently. Numerical experiments show that the new model delivers similar results for easier problems to old models, such as the Badshah-Chen model [4] and the Nguyen-Cai-Zhang-Zheng model [2], and improves on these models in hard cases where objects are nearby or have a

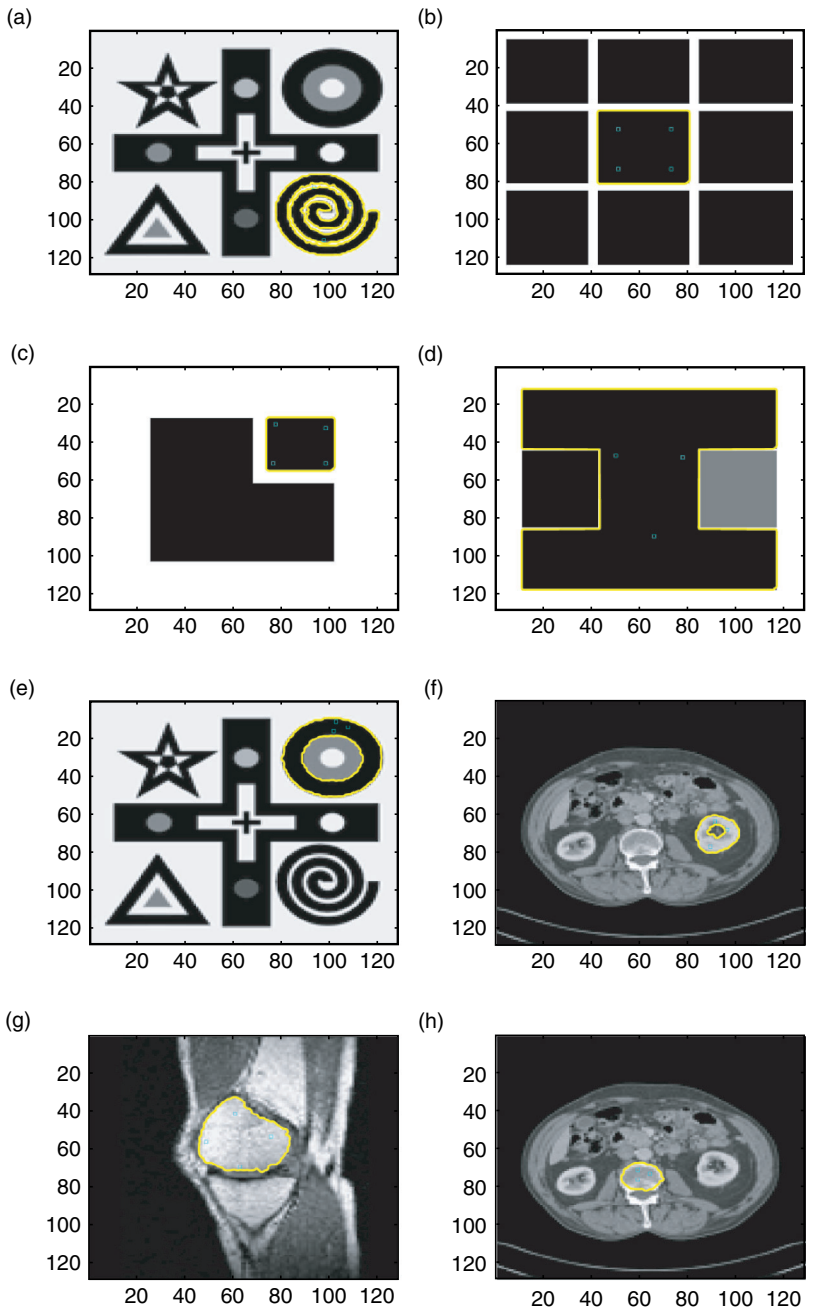

Figure 8. (*continued*)

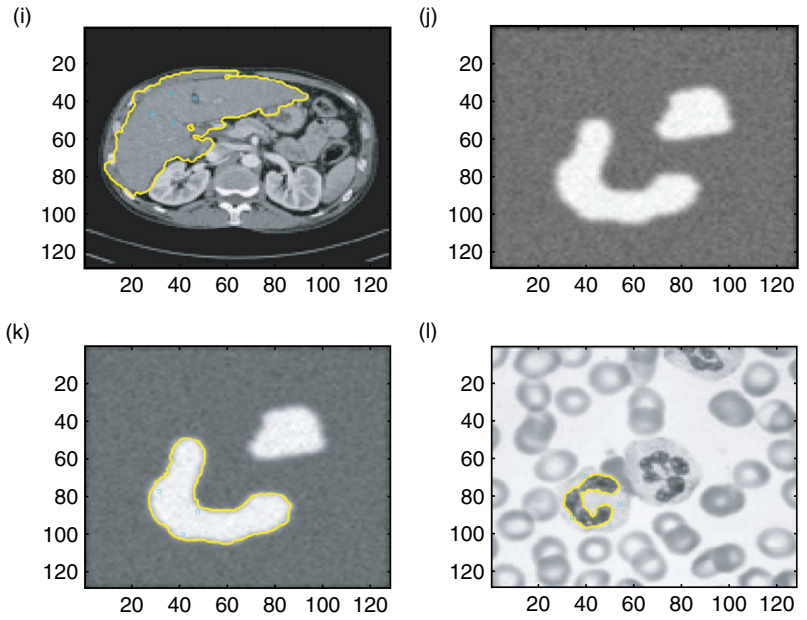

Figure 8. Test Set 3 – Comparative results with Rada-Chen [29] model (a-l) Successful segmentation of different images.

Table 1. Required CPU time for successful selective segmentation for some of the tested images.

	DLSS method	**New method**
Figure	**CPU time**	**CPU time**
Fig. 3(c) (256 × 256)	68.5938	18.7188
Fig. 3(d) (256 × 256)	49.1250	18.9688
Fig. 8(e) (128 × 128)	65.32	36.703
Fig. 8(f) (128 × 128)	69.120	21.890
Fig. 8(l) (128 × 128)	32.601	11.890

small intensity difference. The model produces equally as reliable results for harder problems as the Rada-Chen [29], improving the speed of [29] by at least two times in comparison.

APPENDIX: DERIVATION OF EULER-LAGRANGE EQUATION FOR THE NEW MODEL

Keeping c_1 and c_2 fixed, we minimize (15) with respect to $\phi(x, y)$ to derive briefly the Euler-Lagrange equation. We recall that F is differentiable in the Gâteaux sense at $\phi \in X$ if the limit

$$F'_{\phi}(\psi) = \frac{d}{dh}\Big(F\Big(\phi + h\psi\Big)\Big)\Big|_{h=0} = \lim_{h\to 0}\frac{F\Big(\phi + h\psi\Big) - F(\phi)}{h},$$

is defined for any $\psi \in X$. Coming back to our problem, let us determine the Gâateaux derivative of the energy F_{ϵ} and find the first variation of the functional F_{ϵ} with respect to ϕ such that:

$$\lim_{h\to 0}\frac{d}{dh}\Big(F_{\epsilon}\Big(\phi + h\psi, c_2\Big)\Big) = 0.$$

Using the notation ϕ, u_0 instead of $\phi(x, y)$, $u_0(x, y)$ we have

$$\begin{aligned}
&\mu\frac{d}{dh}\int_{\Omega} g\Big(\Big|\nabla u_0\Big|\Big)\delta_{\epsilon}\Big(\phi + h\psi\Big)\Big|\nabla\Big(\phi + h\psi\Big)\Big| dxdy\Big|_{h=0} \\
&+\frac{d}{dh}\int_{\Omega}\left(\lambda_1\Big|u_0 - c_1\Big|^2 H_{\epsilon}\Big(\phi + h\psi\Big) + \lambda_2\Big|u_0 - c_2\Big|^2\Big(1 - H_{\epsilon}\Big(\phi + h\psi\Big)\Big)\right) \\
&+\nu\left\{\left(\int_{\Omega} H_{\epsilon}\Big(\phi + h\psi\Big) d\xi d\eta - A_1\right)^2 + \left(\int_{\Omega}\Big(1 - H_{\epsilon}\Big(\phi + h\psi\Big)\Big)\right.\right. \\
&\left.\left.\times d\xi d\eta - A_2\Big)^2\right\}\right|_{h=0} = 0
\end{aligned}$$

$$
\begin{aligned}
&\Rightarrow \\
&\mu\int_{\Omega} g\left(\left|\nabla u_0\right|\right)\left(\left|\nabla\left(\phi+h\psi\right)\right|\frac{d}{dh}\delta_{\epsilon}\left(\phi+h\psi\right)dxdy+\delta_{\epsilon}\left(\phi+h\psi\right)\right. \\
&\left.\frac{d}{dh}\left|\nabla\left(\phi+h\psi\right)\right|\right)dxdy\Bigg|_{h=0} \\
&+\int_{\Omega}\left(\lambda_1\left(u_0\left(x,y\right)-c_1\right)^2\delta_{\varepsilon}\left(\phi+h\psi\right)\psi-\lambda_2\left(u_0\left(x,y\right)-c_2\right)^2\right. \\
&\left.\delta_{\varepsilon}\left(\phi+h\psi\right)\psi\right)dxdy+2\nu\int_{\Omega}\left\{\left(\int_{\Omega}H_{\varepsilon}\left(\phi+h\psi\right)d\xi d\eta-A_1\right)\delta_{\varepsilon}\left(\phi+h\psi\right)\psi\right. \\
&\left.-\left(\int_{\Omega}\left(1-H_{\varepsilon}\left(\phi+h\psi\right)\right)d\xi d\eta-A_2\right)\delta_{\varepsilon}\left(\phi+h\psi\right)\psi\,dxdy\right\}\Bigg|_{h=0}=0.
\end{aligned}
$$

Scaling ν and computing the derivatives we have:

$$
\begin{aligned}
&\mu\int_{\Omega} g\left(\left|\nabla u_0\right|\right)\left(\delta_{\epsilon}'\left(\phi\right)\left|\nabla\phi\right|\psi+\delta_{\epsilon}\left(\phi\right)\frac{\nabla\phi}{\left|\nabla\phi\right|}.\nabla\psi\right)dxdy \\
&+\int_{\Omega}\delta_{\epsilon}(\phi)\left(\lambda_1\left(u_0\left(x,y\right)-c_1\right)^2-\lambda_2\left(u_0\left(x,y\right)-c_2\right)^2\right)\psi\;dxdy \\
&\times\nu\int_{\Omega}\delta_{\epsilon}(\phi)\left\{\left(\int_{\Omega}H_{\varepsilon}(\phi)d\xi d\eta-A_1\right)-\left(\int_{\Omega}\left(1-H_{\varepsilon}(\phi)\right)d\xi d\eta-A_2\right)\right\} \\
&\psi dxdy=0
\end{aligned}
$$

or

$$
\begin{aligned}
&\mu\int_{\Omega} g\left(\left|\nabla u_0\right|\right)\delta_{\epsilon}'(\phi)\left|\nabla\phi\right|\psi dxdy+\mu\int_{\Omega} g\left(\left|\nabla u_0\right|\right)\delta_{\epsilon}\left(\phi\right)\frac{\nabla\phi}{\left|\nabla\phi\right|}.\nabla\psi dxdy \\
&+\int_{\Omega}\delta_{\epsilon}(\phi)\left(\lambda_1\left(u_0\left(x,y\right)-c_1\right)^2-\lambda_2\left(u_0\left(x,y\right)-c_2\right)^2\right)\psi dxdy \\
&+\nu\int_{\Omega}\delta_{\epsilon}(\phi)\left\{\left(\int_{\Omega}H_{\varepsilon}\left(\phi\right)d\xi d\eta-A_1\right)-\left(\int_{\Omega}\left(1-H_{\varepsilon}\left(\phi\right)\right)d\xi d\eta-A_2\right)\right\} \\
&\psi dxdy=0
\end{aligned}
\tag{24}
$$

where ψ is a test function of the same type as ϕ. Applying Green's identity

$$
\int_{\Omega} v\nabla\cdot\vec{w}dx=-\int_{\Omega}\nabla v\cdot\vec{w}dx+\int_{\partial\Omega} v\vec{w}\cdot\vec{n}ds
$$

to the second integral of (24) by taking $\psi = v$ and $\vec{w} = g\left(\left|\nabla u_0\right|\right)\dfrac{\delta_\epsilon\left(\phi\right)}{\left|\nabla\phi\right|}\nabla\phi$ for the second integral we rewrite them respectively as

$$\int_\Omega g\left(\left|\nabla u_0\right|\right)\delta_\epsilon\left(\phi\right)\frac{\nabla\phi}{\left|\nabla\phi\right|}\cdot\nabla\psi dx = -\int_\Omega \nabla\cdot\left(g\left(\nabla u_0\right)\frac{\delta_\epsilon\left(\phi\right)}{\left|\nabla\phi\right|}\nabla\phi\right)\psi dxdy$$
$$+\int_{\partial\Omega} g\left(\left|\nabla u_0\right|\right)\frac{\delta_\epsilon\left(\phi\right)}{\left|\nabla\phi\right|}\frac{\partial\phi}{\partial\vec{n}}\psi ds,$$

where $\nabla\phi\cdot\vec{n} = \dfrac{\partial\phi}{\partial\vec{n}}$. Thus equation (24) becomes

$$\begin{cases}\mu\int_\Omega g\left(\left|\nabla u_0\right|\right)\delta_\epsilon'\left(\phi\right)\left|\nabla\phi\right|\psi dxdy + \mu\int_{\partial\Omega} g\left(\left|\nabla u_0\right|\right)\dfrac{\delta_\epsilon\left(\phi\right)}{\left|\nabla\phi\right|}\dfrac{\partial\phi}{\partial\vec{n}}\psi ds\\ -\mu\int_\Omega \nabla\cdot\left(\delta_\epsilon\left(\phi\right)g\left(\left|\nabla u_0\right|\right)\right)\dfrac{\nabla\phi}{\left|\nabla\phi\right|}\psi dxdy\\ +\int_\Omega \delta_\epsilon\left(\phi\right)\left(\lambda_1\left(u_0\left(x,y\right)-c_1\right)^2 - \lambda_2\left(u_0\left(x,y\right)-c_2\right)^2\right)\psi dxdy\\ +\nu\int_\Omega \delta_\epsilon\left(\phi\right)\left(\left(\int_\Omega H_\varepsilon\left(\phi\right)d\xi d\eta - A_1\right) - \left(\int_\Omega\left(1-H_\varepsilon\left(\phi\right)\right)d\xi d\eta - A_2\right)\right)\psi dxdy = 0\end{cases}$$

$$\Rightarrow$$

$$\begin{cases}\mu\int_\Omega g\left(\left|\nabla u_0\right|\right)\delta_\epsilon'\left(\phi\right)\left|\nabla\phi\right|\psi dxdy + \mu\int_{\partial\Omega} g\left(\left|\nabla u_0\right|\right)\dfrac{\delta_\epsilon\left(\phi\right)}{\left|\nabla\phi\right|}\dfrac{\partial\phi}{\partial\vec{n}}\psi ds -\\ \mu\int_\Omega \delta_\epsilon\left(\phi\right)\nabla\cdot\left(g\left(\left|\nabla u_0\right|\right)\dfrac{\nabla\phi}{\left|\nabla\phi\right|}\right)\psi dxdy - \mu\int_\Omega \delta_\epsilon'\left(\phi_L\right)g\left(\left|\nabla u_0\right|\right)\nabla\phi\cdot\dfrac{\nabla\phi}{\left|\nabla\phi\right|}\psi dxdy\\ +\int_\Omega \delta_\epsilon\left(\phi\right)\left(\lambda_1\left(u_0\left(x,y\right)-c_1\right)^2 - \lambda_2\left(u_0\left(x,y\right)-c_2\right)^2\right)\psi dxdy\\ \nu\int_\Omega \delta_\epsilon\left(\phi\right)\left(\left(\int_\Omega H_\epsilon(\phi)d\xi d\eta - A_1\right) - \left(\int_\Omega\left(1-H_\varepsilon(\phi)\right)d\xi d\eta - A_2\right)\right)\psi dxdy = 0.\end{cases}$$

This gives

$$\begin{cases} -\mu\int_\Omega \delta_\epsilon(\phi)\nabla\cdot\left(g\left(\left|\nabla u_0\right|\right)\dfrac{\nabla\phi}{\left|\nabla\phi\right|}\right)\psi dxdy+\mu\int_{\partial\Omega} g\left(\left|\nabla u_0\right|\right)\dfrac{\delta_\epsilon(\phi)}{\left|\nabla\phi\right|}\dfrac{\partial\phi}{\partial\vec{n}}\psi ds+ \\ \int_\Omega \delta_\epsilon(\phi)\left(\lambda_1\left(z-c_1\right)^2-\lambda_2\left(z-c_2\right)^2\right)\psi dxdy+ \\ \nu\int_\Omega \delta_\epsilon(\phi)\left[\left(\int_\Omega H_\varepsilon(\phi)\,d\xi d\eta-A_1\right)-\left(\int_\Omega\left(1-H_\varepsilon(\phi)\right)d\xi d\eta-A_2\right)\right]\psi dxdy=0. \end{cases}$$

Since $W=g(|\nabla u_0|)$ the Euler-Lagrange equation for ϕ can be derived:

$$\begin{aligned} &\mu\delta_\epsilon(\phi)\nabla\cdot\left(W\frac{\nabla\phi}{\left|\nabla\phi\right|}\right)+\delta_\epsilon(\phi)\left\{-\lambda_1\left(u_0(x,y)-c_1\right)^2+\lambda_2\left(u_0(x,y)-c_2\right)^2\right. \\ &\left.-\nu\left[\left(\int_\Omega H_\varepsilon(\phi)\,dxdy-A_1\right)-\left(\int_\Omega\left(1-H_\varepsilon(\phi)\right)dxdy-A_2\right)\right]\right\}=0 \end{aligned} \tag{25}$$

in Ω, where the boundary condition $\mu g\left(\left|\nabla u_0\right|\right)\dfrac{\delta_\epsilon(\phi)}{\left|\nabla\phi\right|}\dfrac{\partial\phi}{\partial\vec{n}}=0$ reduces to the Neumann boundary condition. Equation (25) can be rewritten as:

$$\begin{aligned} &\delta_\epsilon(\phi)\left\{\mu\nabla.\left(W\frac{\nabla\phi}{\left|\nabla\phi\right|}\right)-\left[\lambda_1\left(u_0(x,y)-c_1\right)^2-\lambda_2\left(u_0(x,y)-c_2\right)^2\right]\right. \\ &\left.-\nu\left[\left(\int_\Omega H dxdy-A_1\right)-\left(\int_\Omega\left(1-H\right)dxdy-A_2\right)\right]\right\}=0, \end{aligned} \tag{26}$$

in Ω with $\left.\dfrac{\partial\phi}{\partial\vec{n}}\right|_{\partial\Omega}=0.$

REFERENCES

[1] R. Adams and L. Bischof. Seeded region growing. *IEEE Trans. Pattern Anal. Mach. Intell.*, 16(6):641–647, June 1994.

[2] Nguyen Thi Nhat Anh, Jianfei Cai, Juyong Zhang, and Jianmin Zheng. Robust interactive image segmentation using convex active contours. *IEEE Transactions on Image Processing*, 21(8):3734–3743, 2012.

[3] G. Aubert and P. Kornprobst. *Mathematical problems in image processing: Partial differential Equations and the Calculus of Variations*. Springer, 2001.

[4] N. Badshah and Ke Chen. Image selective segmentation under geometrical constraints using an active contour approach. *Commun. Comput. Phys.*,

7(4):759–778, 2009.

[5] X. Bai and G. Sapiro. A geodesic framework for fast interactive image and video segmentation and matting. *in IEEE ICCV*, pages 1–8, 2007.

[6] Xavier Bresson, Selim Esedoglu, Pierre Vandergheynst, Jean-Philippe Thiran, and Stanley Osher. Fast global minimization of the active contour/snake model. *Journal of Mathematical Imaging and Vision*, 28:151–167, 2007.

[7] V. Caselles, R. Kimmel, and G. Sapiro. Geodesic active contours. *International Journal of Computer Vision*, 22(1):61–79, 1997.

[8] Tony F. Chan, B.Yezrielev Sandberg, and Luminita A. Vese. Active contours without edges for vector-valued images. *Journal of Visual Communication and Image Representation*, 11(2):130 – 141, 2000.

[9] Tony F. Chan and Luminita A. Vese. Active contours without edges, 1998.

[10] Tony F. Chan and Luminita A. Vese. Active contours without edges. *IEEE Transactions on Image Processing*, 10(2):266–277, 2001.

[11] Dorin Comaniciu, Peter Meer, and Senior Member. Mean shift: A robust approach toward feature space analysis. *IEEE Transactions on Pattern Analysis and Machine Intelligence*, 24:603–619, 2002.

[12] D. Cremers and C. Schnörr. Statistical shape knowledge in variational motion segmentation. *Image and Vision Comp.*, 21(1):77–86, 2003.

[13] Stuart Geman and Donald Geman. Stochastic relaxation, gibbs distributions and the bayesian restoration of images. *IEEE Transactions on Pattern Analysis and Machine Intelligence*, 6(6):721–741, 1984.

[14] Tom Goldstein, Xavier Bresson, and Stanley Osher. Geometric applications of the split bregman method: Segmentation and surface reconstruction. *J. Sci. Comput.*, 45(1–3):272–293, 2010.

[15] C. Gout and C. Le Guyader. Segmentation of complex geophysical structures with well data. *Computational Geosciences*, 10(4):361–372, 2006.

[16] C. Gout, C. Le Guyader, and L. A. Vese. Segmentation under geometrical consitions with geodesic active contour and interpolation using level set methods. *Numerical Algorithms*, 39:155–173, 2005.

[17] L. Grady. Random walks for image segmentation. *IEEE Transactions on Pattern Analysis and Machine Intelligence*, 28(11):1768 1783, 2006.

[18] C. Le Guyader and C. Gout. Geodesic active contour under geometrical conditions theory and 3d applications. *Numerical Algorithms*, 48:105–133, 2008.

[19] Steve Hanov. Wavelets and edge detection (preprint). *steve-hanov.ca/cs698_wavelet_project.pdf*, April 2006.

[20] Michael Kass, Andrew Witkin, and Demetri Terzopoulos. Snakes: Active contour models. *International Jurnal of Computer Vision*, 1(4):321–331, 1988.

[21] Y. Leclerc. Region growing using the mdl principle. *In: DAPPRA Image Understanding Workshop*, 1990.

[22] C. Li, C. Xu, C. Gui, and M. D. Fox. Level set evolution without reinitialization: A new variational formulation. *IEEE Computer Society Conference on Computer Vision and Pattern Recognition*, 1:430–436, 2005.

[23] T. Lu, P. Neittaanmaki, and X. C. Tai. A parallel splitting-up method for partial differential equations and its application to navier-stokes equations. *RAIRO Mathematical Modelling and Numerical Analysis*, 26(6):673–708, 1992.

[24] J. Malik, Th. Leung, and J. Shi. Contour and texture analysis for image segmentation. *International Journal of Computer Vision*, 43:7–27, 2001.

[25] Stephane Mallat. *A Wavelet Tour Of Signal Processing*. Academic Press, USA, 1998.

[26] D. Mumford and J. Shah. Optimal approximation by piecewise smooth functions and associated variational problems. *Communications on Pure Applied Mathematics*, 42:577–685, 1989.

[27] S. Osher and R. Fedkiw. *Level Set Methods and Dynamic Implicit Surfaces*. Springer, Berlin, 2003.

[28] Stanley Osher and James A. Sethian. Fronts propagating with curvature dependent speed: Algorithms based on hamilton-jacobi formulations. *Journal of Computational Physics*, 79(1):12–49, 1988.

[29] L. Rada and Ke Chen. A new variational model with dual level set functions for selective segmentation. *Commun. Comput. Phys.*, 12(1):261–283, 2012.

[30] C. Rother, V. Kolmogorov, and A. Blake. Grabcut: Interactive foreground extraction using iterated graph cuts. *in ACM SIGGRAPH*, 2004.

[31] G. Sapiro, R. Kimmel, and V. Casells. Object detection and measurements in medical images via geodesic deformable contours. In F. L. Bookstein & W. D. Green R. A. Melter, A. Y. Wu, editor, *Society of Photo-Optical Instrumentation Engineers (SPIE) Conference Series*, volume 2573 of *Society of Photo-Optical Instrumentation Engineers (SPIE) Conference Series*, pages 366–378, 1995.

[32] D. Sen and S. K. Pal. Histogram thresholding using fuzzy and rough measures of association error. *Image Processing, IEEE Transactions on*, 18(4):879–888, 2009.

[33] J. A. Sethian. *Level Set Methods and Fast Marching Methods: Evolving Interfaces in Computational Geometry, Fluid Mechanics, Computer Vision, and Materials Science*. Cambridge University Press, 1999.

[34] Sheshadri R. Thiruvenkadam, Tony F. Chan, and Byung-Woo Hong. Segmentation under occlusions using selective shape prior. In *Proceedings of the 1st international conference on Scale space and variational methods in computer vision*, SSVM'07, pages 191–202, Berlin, Heidel-berg, 2007. Springer-Verlag.

[35] N. Valliammal and S. N. Geethalakshmi. Performance analysis of various leaf